Macromolecules

Article

pubs.acs.org/Macromolecules

Role of pH on the Compaction Energies and Phase Behavior of Low Generation PAMAM–DNA Complexes

Min An, James M. Hutchison, Sean R. Parkin, and Jason E. DeRouchey*

Department of Chemistry, University of Kentucky, Lexington, Kentucky 40506, United States

ABSTRACT: Cationic polymers are capable of spontaneously condensing DNA into complexes suitable for nonviral gene therapy. The precisely defined molecular weights and highly symmetric surface chemistries of dendrimers, such as poly(amidoamine) (PAMAM), have made them attractive alternatives to conventional linear polymers for DNA delivery applications. In this paper, we use small-angle X-ray scattering (SAXS) coupled with osmotic stress to directly measure the effect of pH on the packaging and forces in low generation (G0 and G1) PAMAM–DNA complexes or dendriplexes. Because of the presence of both primary and tertiary amines with differing pK_as, PAMAM changes its net charge with pH. We show that changing the pH at condensation results in large differences in the packaging and intermolecular forces in PAMAM dendriplexes. Both dendrimer/DNA systems show a large increase in attractions with decreasing pH scaling linearly with the inverse of the dendrimer charge, while repulsions in the system are nearly unaffected. pH also greatly influences the resulting phase behavior and salt sensitivities of the PAMAM–DNA complexes. With increasing salt concentration, a discontinuous phase transition is observed from a hexagonal packaging of DNA helices to a more loosely ordered cholesteric phase for both PAMAM dendriplex systems studied. The phase transition occurs at a critical salt concentration, c^*, that is dependent on both the PAMAM generation number and the pH. When normalized by c^*, this salt-induced melting transition is found to be universal for a given dendrimer/DNA system.

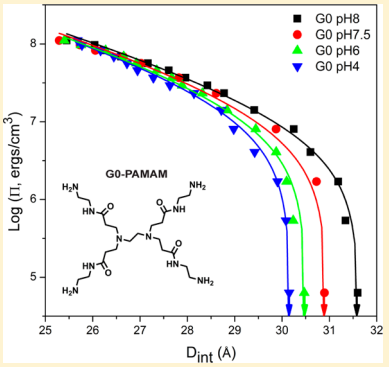

INTRODUCTION

Gene delivery is a complicated multistep process with the ultimate goal of replacing a defective gene sequence with a corrected version of that gene. Currently gene delivery focuses on either viral or nonviral vectors to deliver nucleic acids into cells in a safe and effective manner.[1,2] Viral vectors suffer from potential limitations including broad tropism, limited DNA packaging capacity, and difficulties in large-scale production, thus motivating studies on nonviral alternatives.[3] Many nonviral systems rely on cationic polymers to both package DNA and facilitate the delivery of genes *in vivo*.[4] Possible benefits of cationic polymers over viral vectors include low immunogenicity and ease of chemical modification.[5,6] In recent years, cationic dendrimers have become attractive alternatives to traditional linear cationic systems. Dendrimers are hyperbranched macromolecules with near uniform polydispersity and well-defined surface chemistries. Typically, dendrimers are built in an iterative fashion with concentric branching units stemming from a central core. With each growth step, or generation, a doubling of the reactive surface groups of the preceding generation is achieved. Dendrimers have distinct advantages over linear cationic polymers which typically suffer from inherent problems such as chain polydispersity and random attachment of functional domains. DNA condensed with commercially available cationic dendrimers such as poly(amidoamine) (PAMAM) and polypropylenimine (PPI) dendrimers are the most studied dendrimer–DNA, or dendriplex, systems for gene delivery. Both dendrimers are capable of condensing DNA and protecting nucleic acids from restriction nucleases.[7−9]

Successful gene therapy requires first a packaging of DNA through complexation of the cationic agent to DNA, and then after successful transport to the cell of interest, the DNA must unpackage. Both packaging and unpackaging are dependent on the structure and forces within the polycation–DNA complex. For successful application of dendriplexes as a therapeutic, there is a need to characterize the resulting structure and compaction energies within dendrimer–DNA complexes. Theoretical studies and simulations on semiflexible polyelectrolyte interacting with charged spheres have predicted that wrapping of the polymer chain around the sphere to form so-called "beads on a string" (BOS) structures are possible.[10,11] Similar structures have also been predicted for DNA complexing with high generation dendrimers.[12−15] One of the first experimental studies by Evans et al. showed dendriplexes to have a mesomorphic nature forming either 2D hexagonal or square columnar mesophases with G4 and G5 PPI dendrimers.[16] Further experiments with different chemistries and generation of dendrimers have shown highly conflicting results in terms of internal structure upon DNA complexation. Dendriplex structures with square, tetragonal, and hexagonal packaged columnar mesophases, as well as DNA wrapping and BOS structures, have all been reported as observed by small-

Received: October 9, 2014
Revised: November 20, 2014
Published: December 5, 2014

angle X-ray and neutron scattering (SAXS/SANS), atomic force microscopy (AFM), and single molecule experiments.[17−28]

Using osmotic force coupled to SAXS, we are able to directly measure packaging and forces within ordered DNA assemblies. In an earlier study, we compared DNA packaged by low generation (G0 and G1) PAMAM dendrimers to linear polyarginines (R_4 and R_8) which carried the same number of positive charges at neutral pH: +4 and +8, respectively.[29] The forces in low generation PAMAM−DNA complexes are well described by exponential functions with fixed 2.5 and 5 Å decay lengths. This form is consistent with previous work on forces within DNA condensed with $Co(NH_3)_6$ and a wide variety of linear polycations.[30−33] Using force measurements to quantitate the contributions to the overall forces, we showed that DNA condensed by the hyperbranched dendrimers display significantly different physical behavior in comparison to linear cation−DNA assemblies. These differences arise due to PAMAM having both increased repulsions and significantly weakened attractions when compared to linear cations of the same net charge. We argue these differences likely arise due to dendrimers being unable to bind to DNA within grooves, as has been suggested for linear cations, but rather must use alternative binding modes such as bridging to induce condensation.

We report here on studies performed to better understand the effect of pH on low generation PAMAM dendriplexes. We have systematically investigated packaging and compaction energies within G0- and G1-PAMAM dendriplexes condensed between pH 4 and pH 8. We show that changing the pH at condensation has significant effects on the observed structure and phase behavior of the resulting PAMAM/DNA complexes. Because of the presence of primary and tertiary amines in PAMAM with varying pK_as, tuning pH directly alters the total charge of the dendrimers. At low pH, or higher net dendrimer charge, more tightly packaged DNA is achieved. Despite variations with pH in the packaging density achieved at equilibrium, or zero applied pressure, we see a convergence of the force stress curves at high osmotic pressure for each dendriplex system. Fits to the force curves indicate that the repulsive contributions for a given PAMAM/DNA system are relatively insensitive to pH while the attractions vary greatly, scaling linearly with the inverse net dendrimer charge. Lastly, we examined the salt dependence of the phase behavior in PAMAM dendriplexes as a function of the pH at condensation. A universal phase behavior is observed for both G0- and G1-PAMAM dendriplexes with a discontinuous phase transition observed above a critical salt concentration, c^*. This critical salt concentration is sensitive to both dendrimer generation and pH.

MATERIALS AND METHODS

Materials. Low generation PAMAM dendrimers (generations 0 and 1, ethylenediamine core, amine-terminated polyamidoamine) were purchased from Sigma-Aldrich (St Louis, MO). Before use, methanol was removed using a Labconco Centrivap at reduced pressure. Dendrimers were subsequently dissolved in appropriate buffer solution, and the final pH was adjusted with NaOH or HCl to the desired pH value (from pH = 4 to 8). Bioultra grade poly(ethylene glycol) (PEG, 8 kDa) was obtained from Fluka Chemical Co. and used without further purification. Highly polymerized calf-thymus (CT) DNA sodium salt (molecular weight ∼10−15 million Da) was purchased from Sigma-Aldrich. High-molecular-weight chicken blood (CB) DNA (molecular weight >5 × 10^6 Da) was prepared and purified from adult chicken whole blood as described previously.[34] CT and CB DNA were further purified by phenol/chloroform extraction to remove excess proteins followed by ethanol precipitation before use. After purification, both DNAs were extensively dialyzed against 1 mM EDTA solution. The successful removal of protein from both CB and CT DNA was verified by measuring the ratio of absorbance at 260 and 280 nm of DNA solutions and found to be satisfactory with values exceeding 1.8.

Sample Preparation. DNA was observed to spontaneously precipitate in the presence of both G0- and G1-PAMAM for all pHs used in this study. In preparing samples, both the DNA (CB or CT DNA) and dendrimer (G0 or G1) stock solutions were first separately dissolved in an appropriate 10 mM pH buffer. After dissolution, these stock solutions were further buffered with HCl or NaOH to achieve the desired final pH (pH ± 0.1). Buffers used were 10 mM sodium acetate solution for pH 4, 10 mM MES solution for pH 6, and 10 mM Tris-HCl for pH 8 and pH 7.5. The double-helix structure of DNA is known to be stable over this pH range. Condensed DNA samples for X-ray scattering were subsequently prepared in one of two ways. Concentrated PAMAM stock solutions were added to 1 mg/mL calf-thymus (CT) or chicken blood (CB) DNA in 10 mM pH buffer in a stepwise fashion. Each addition was mixed thoroughly before adding additional PAMAM, and the process continued until all DNA was precipitated. Alternatively, a single aliquot of condensing cations was added to DNA to an equivalent final concentration. The final cation amine to DNA phosphate ratio was approximately 1.2 at the end point. The resulting fibrous PAMAM−DNA samples were then centrifuged for 10 min and transferred to a 10 mM pH buffered PEG-salt solution and allowed to equilibrate ∼2 weeks before X-ray analysis. X-ray scattering profiles did not depend on the type of DNA used or the sample method employed to prepare the DNA precipitate. In all samples, a small excess PAMAM concentration was maintained in the PEG-salt bathing solution to ensure cation concentration was above the critical concentration for these cations as previously determined. The observed spacing between helices does not depend on the excess cation concentration in the bath over an approximately 2−5-fold concentration range. X-ray scattering patterns were not observed to change even after several months of storage.

Osmotic Pressure. The method for direct force measurements by osmotic pressure has been described previously in detail.[30,35] In brief, condensed DNA arrays equilibrate against a bathing PEG polymer solution with a known osmotic pressure. PEG chains are too large to enter into the condensed DNA phase, thus providing a direct osmotic pressure on the DNA condensates. In these samples, small molecules including water and salt are free to exchange between the PEG and condensed DNA phases. After equilibration, the osmotic pressures in both phases are the same. Osmotic pressures of the bathing PEG solutions were measured directly using a Wescor Vapro vapor pressure osmometer (model 5660). In the condensed state with low generation PAMAM, the DNA rods are found to be packaged in a hexagonal array for all pHs at low salt conditions. Using small-angle X-ray scattering (SAXS), the interaxial spacing between DNA rods (D_{int}) can be determined as a function of the osmotic pressure from the Bragg scattering of X-rays to obtain force−separation curves as described below.

X-ray Scattering. X-ray scattering experiments were performed using graded-multilayer focused CuKα radiation (1.54 Å) from a Nonius FR-591 rotating anode fine-focus X-ray generator operating at 45 kV and 20 mA. Samples were sealed in a sample cell with a bath of equilibrating PEG solution and mounted in a sample holder at room temperature. The flight path from the sample to detector was filled with helium gas to minimize air scatter, and the primary beam was collimated by a fine aperture beam tunnel. Diffraction patterns were recorded by a SMART 6000 CCD detector with phosphor optimized for Cu Kα radiation. Fit2D and Origin 8.0 software were used to analyze all images. Calibration of the SAXS sample-to-detector distance was performed using silver behenate powder and found to be 23.2 cm. Bragg scattering peaks were used to determine interaxial DNA−DNA spacings. Bragg spacings are calculated as $D_{Br} = 2\pi/q_{Br}$, where q_{Br} is the scattering vector, q (defined as $q = (4\pi/\lambda)\sin(\theta)$,

dx.doi.org/10.1021/ma5020808 | Macromolecules 2014, 47, 8768−8776

where 2θ is the scattering angle), which corresponds to the maximum in the scattering. For a hexagonal lattice, the relationship between the Bragg spacing and the actual interaxial distance between helices (D_{int}) is calculated as $D_{int} = (2/\sqrt{3})D_{Br}$. For different samples equilibrated under the same PEG-salt conditions, D_{int} values were reproducible to within ~0.1 Å. X-ray scattering patterns were reproducible over several months of storage, and there was no significant sample degradation due to X-ray exposure. Typical exposure times were 120 s.

Force Analysis. G0- and G1-PAMAM are both able to condense DNA spontaneously *in vitro* into hexagonal DNA arrays with a finite separation at equilibrium between the DNA helices. We use the osmotic stress technique to directly probe the intermolecular forces between the PAMAM condensed DNA. Previous studies indicate that DNA–DNA forces are well described by two exponentials at close interhelical distances.[30−33] We fit the osmotic pressure Π versus interhelical spacing D_{int} curves to a double-exponential equation with variable attractive and repulsive pre-exponential factors A and R:

$$\Pi(D) = \Pi_R(D) + \Pi_A(D) = Re^{-2D/\lambda} + Ae^{-D/\lambda} \quad (1)$$

with the long-range decay length λ fixed at 5 Å. This form and decay length constraint are the result of prior experiments that combined osmotic stress measurements with magnetic tweezing experiments to independently evaluate the attractive and repulsive contributions to the free energies at equilibrium for several common cationic condensing agents.[31]

Equation 1 with λ = 5.0 Å has been used previously and gives very good fits for a variety of condensing agents including G0- and G1-PAMAM dendrimer.[29,32,33,36] Results are only slightly dependent on the decay length λ over the range of ±0.5 Å. For condensed DNA systems, the coefficients A and R are connected through the interhelical equilibrium distance, D_{eq}, since $\Pi(D_{eq}) = 0$, resulting in a fitting equation with only a single variable, R.

$$\log(\Pi(D)) = \log(R) - \frac{2D}{2.303\lambda} + \log(1 - e^{-(D_{eq}-D)/\lambda}) \quad (2)$$

With hexagonal packing of DNA, the repulsive and attractive free energy contributions per DNA base pair can be calculated at any spacing D by integrating Π dV for each exponential from ∞ to D as

$$\frac{\Delta G_R(D)}{kT} = \frac{\sqrt{3}\,b(\lambda/2)(D + \lambda/2)}{kT}\Pi_R(D) \quad (3)$$

and

$$\frac{\Delta G_A(D)}{kT} = \frac{\sqrt{3}\,b\lambda(D + \lambda)}{kT}\Pi_A(D) \quad (4)$$

where b, the linear spacing between DNA base pairs, is 3.4 Å.

RESULTS

Role of pH on Intermolecular Forces in PAMAM–DNA. The pH at condensation plays a significant role in changing the observed DNA packaging for both G0- and G1-PAMAM/DNA complexes at equilibrium. We previously observed that the pH at condensation has a much stronger effect on PAMAM/DNA packaging compared to changing the pH after dendriplex formation.[29] For all samples discussed in this paper, both dendrimer and DNA stock solutions were first made separately in pH appropriate 10 mM buffers. Stock solutions were subsequently titrated with concentrated HCl or NaOH to achieve the desired final pH. Dendrimer–DNA complexes were then precipitated by mixing the separate stock solutions and maintained at the same pH with buffer.

Osmotic stress experiments coupled to small-angle X-ray scattering (SAXS) were performed to investigate the effect of pH on the compaction energies and intermolecular forces in low generation PAMAM condensed DNA. Figures 1 and 2 show osmotic stress force curves for DNA condensed with G0- and G1-PAMAM, respectively, as a function of the pH at condensation. Plotted are log osmotic pressure Π versus interaxial spacings (D_{int}) between DNA helices. Arrows indicate the interaxial spacings for these PAMAM/DNA complexes in the absence of applied osmotic pressure. All force curves are well described by the double-exponential formalism described above. Solid lines are fits of the data to eq 2 with decay length λ fixed at 5.0 Å. These fits allow us to separate the net force into its attractive and repulsive contributions to the free energies.

At all pHs studied, both G0- and G1-PAMAM were able to spontaneously condense DNA consistent with a hexagonal packaging of the DNA at equilibrium (i.e., Π = 0). At equilibrium, we see a pH-dependent interaxial DNA spacing

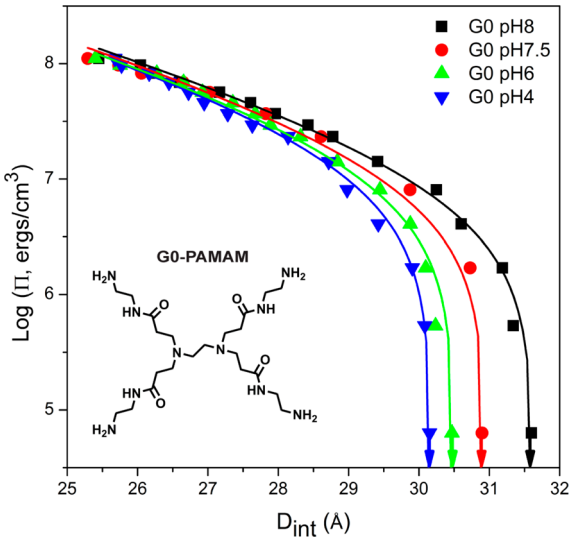

Figure 1. Osmotic stress force curves are shown for G0-PAMAM/DNA as a function of pH at condensation. DNA and dendrimer were mixed and maintained at the pH indicated. Arrows indicate the equilibrium spacing in the absence of applied osmotic pressure. Solid lines are fits of the data to eq 2 with λ = 5 Å.

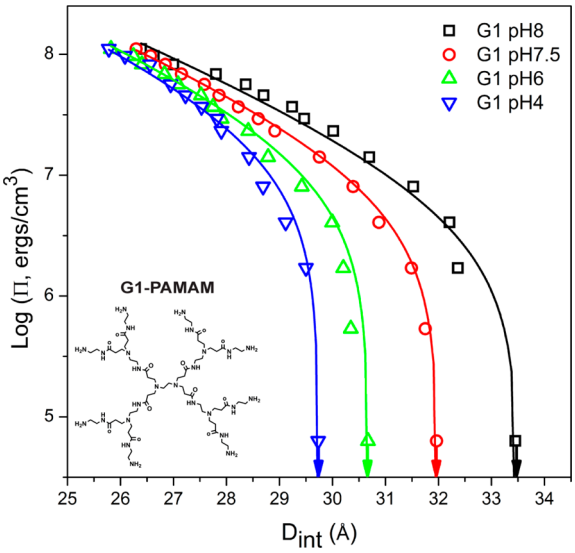

Figure 2. Osmotic stress force curves are shown for G1-PAMAM/DNA as a function of pH at condensation. Samples were mixed and maintained at the pH indicated. Arrows indicate the equilibrium spacing in the absence of applied osmotic pressure. Solid lines are fits of the data to eq 2 with λ = 5 Å.

dx.doi.org/10.1021/ma5020808 | Macromolecules 2014, 47, 8768–8776

Table 1. Equilibrium Interhelical Spacings, ±0.1 Å, from SAXS Measurements and Repulsive and Attractive Force Component Contributions to Osmotic Pressures and Free Energies (±5%) for G0- and G1-PAMAM Condensed DNA at Different pHs[a]

cation	pH	D_{eq} (Å)	Π_R(25 Å) (10^8 erg cm^{-3})	Π_A(25 Å) (10^8 erg cm^{-3})	ΔG_R(25 Å) kT per base pair	$-\Delta G_A$(25 Å) kT per base pair	$-\Delta G_{NET}(D_{eq})$ kT per base pair
G0-PAMAM	4	30.1	2.30	0.82	2.27	1.76	0.39
	6	30.5	2.25	0.75	2.22	1.61	0.34
	7.5	30.9	2.29	0.70	2.26	1.50	0.29
	8	31.6	2.32	0.62	2.29	1.33	0.23
G1-PAMAM	4	29.7	2.72	1.06	2.69	2.28	0.55
	6	30.7	2.61	0.84	2.58	1.81	0.37
	7.5	32.0	2.67	0.66	2.64	1.42	0.23
	8	33.5	2.83	0.52	2.79	1.11	0.14

[a]All values are calculated from fits to force curves and shown for 25 Å separations or 5 Å water between DNA helices. Net free energy gain (ΔG_{NET}) evaluated at the equilibrium spacing, D_{eq}, is also given.

(D_{eq}) as tabulated in Table 1 with the tightest packaging observed at low pH. D_{eq} in G0-PAMAM/DNA ranges from 30.1 to 31.6 Å (±0.1 Å) for pH 4−8. DNA condensed with G1-PAMAM, with its larger number of total amines, has an even larger range of D_{eq} spacings from 29.7 to 33.5 Å (±0.1 Å) over the same pH range.

Role of pH on Free Energy Contributions in G0- and G1-PAMAM−DNA Condensates. Also given in Table 1 are the pH-dependent osmotic pressure contributions, Π_R and Π_A, and the repulsive and attractive free energy contributions, ΔG_R and ΔG_A, as determined from the osmotic stress force curve fits and evaluated at 25 Å or equivalently 5 Å water separating DNA helices. As shown, we see a continuous decrease in D_{eq} as pH is lowered. This increase in packaging density could be accounted for by a decreasing repulsive force and/or an increasing attraction with pH. Free energy contributions for both G0- and G1-PAMAM dendrimers show that these systems have nearly pH-insensitive repulsive contributions. The attractive free energy contributions, however, are highly pH dependent with the largest values measured at low pH. Lastly in Table 1, we also show the pH dependence of the net ΔG per DNA base pair calculated at equilibrium. Here, $\Delta G_{NET}(D_{eq}) = -(\Delta G_A(D_{eq}) + \Delta G_R(D_{eq}))$. The calculated $\Delta G_{NET}(D_{eq})$ are small (<0.6 kT/DNA bp), consistent with experimentally measured values from magnetic tweezing experiments of DNA condensation with multivalent cations.[31]

PAMAM dendrimers have both primary and tertiary amine groups with different pK_as, resulting in a pH-dependent protonation state. G0-PAMAM has 4 primary and 2 tertiary amines while G1-PAMAM has 8 primary and 6 tertiary amines. At neutral pH, PAMAM's tertiary amines carry almost no charge, but complete protonation of the primary amine groups results in +4 and +8 total charge for G0- and G1-PAMAM, respectively. Lowering the pH further increases the net PAMAM charge due to protonation of the tertiary amines. For pH above 7, primary amines can be deprotonated, thus decreasing the net charge. Using the degree of protonation estimates of Cakara et al.,[37] we calculate to a first approximation the nominal net charge of G0-PAMAM to be approximately +3.5 to +5.1 and G1-PAMAM to be approximately +7 to +13 over the range of pH 8 to pH 4. Figure 3 shows how the measured attractive and repulsive free energies depend on the estimated inverse charge of the PAMAM dendrimers, N. The repulsive free energies for G1-PAMAM/DNA are measured to be about 18% greater than G0-PAMAM/DNA at all pHs measured. Both dendrimers however show only slight variations (<4%) in their repulsive force magnitude as a function of the dendrimer net charge, N. In contrast, attractive free energies vary greatly with N. For both G0- and G1-PAMAM condensed DNA, the ΔG_A scales approximately linearly with the inverse of the estimated residual charge of the dendrimer, N. This $1/N$ behavior in attractions is similar to homologous linear cations, such as alkylamines, lysines, and arginines, studied previously.[32,33]

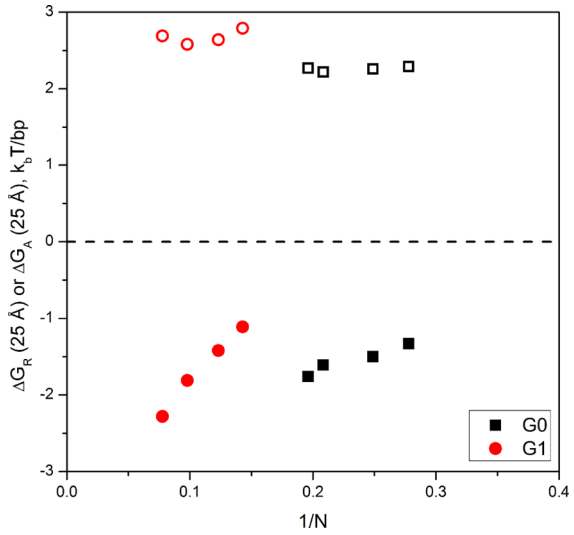

Figure 3. Dependence of the free energy contributions, ΔG_R (open) and ΔG_A (filled), evaluated at 25 Å for G0- and G1-PAMAM condensed DNA as a function of the inverse net charge, N, of the PAMAM estimated for the various pHs used in this study.

pH Effects on Salt Stability and Phase Behavior in PAMAM−DNA. A summary of the observed changes in the Bragg spacings (D_{Br}) with increasing added NaCl salt concentration is given in Figure 4 for G0-PAMAM/DNA and G1-PAMAM/DNA condensed at pH 4−8. Here, we plot the dependence of the Bragg reflections to avoid complications with possible phase transitions that may occur at high salt. Figures 4A and 4B show the DNA Bragg spacings for G0- and G1-PAMAM dendriplexes as a function of added NaCl salt concentration. Figures 4C and 4D show the absolute change in the Bragg spacing compared to no added salt ($D_{Br}-D_{Br,eq}$) for G0- and G1-PAMAM/DNA, respectively. For all pHs in both G0- and G1-PAMAM/DNA, we observe swelling of the Bragg spacings with increasing added NaCl concentration. The swelling behavior is highly dependent not only on which dendrimer was used to condense DNA but also on the pH at condensation. Where Bragg scattering is observed, we observe

dx.doi.org/10.1021/ma5020808 | Macromolecules 2014, 47, 8768−8776

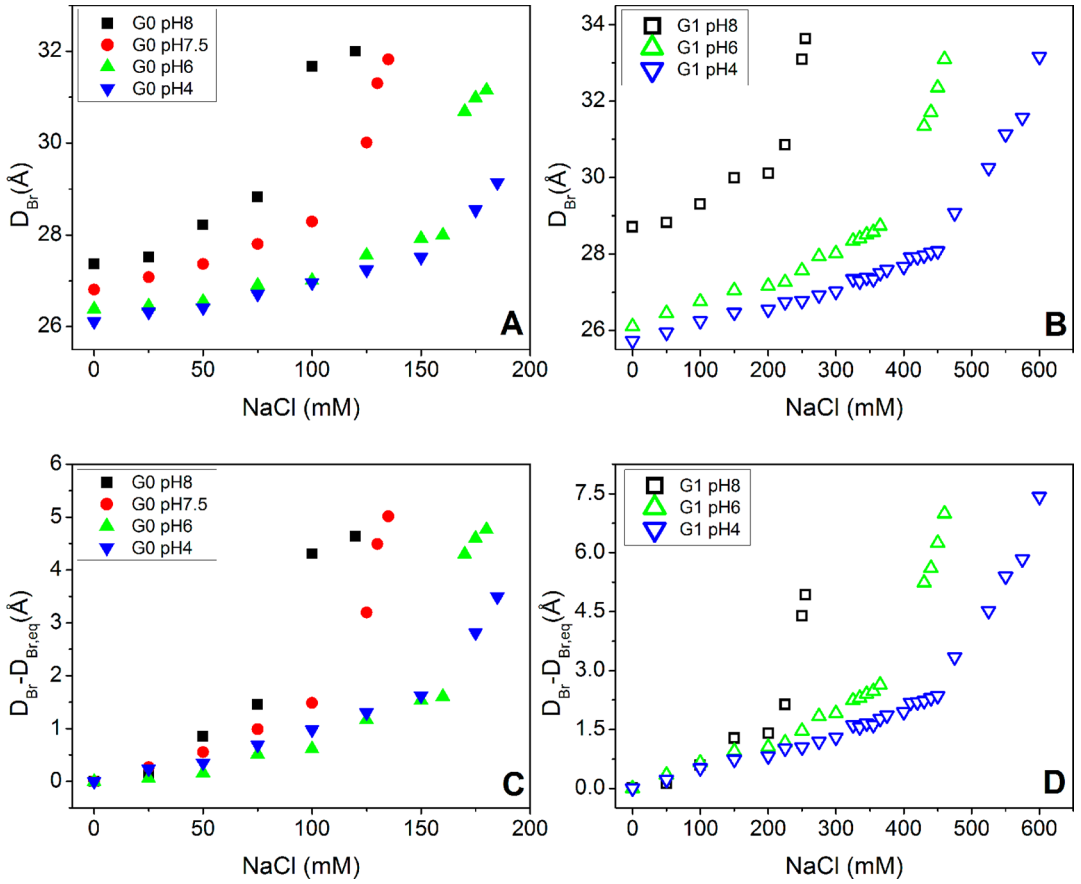

Figure 4. (A) Bragg spacing dependence as a function of added NaCl concentration for G0-DNA and (B) G1-DNA condensed systems at different pHs. (C) and (D) plot the change in the Bragg spacing relative to D_{Br} in 10 mM monovalent buffer without added salt ($D_{Br,eq}$). The equilibrium solutions show no Bragg scattering at the next higher salt concentration in each series.

two regimes with different slopes, or rates of swelling, with added salt. We define a critical salt concentration, c^*, as the salt concentration where these two slopes cross. c^* for G0-PAMAM is observed to change from ~75 mM for DNA condensed at pH 8 to 150 mM NaCl for DNA condensed at pH 4. Similarly, G1-PAMAM dendriplexes have c^* values ranging from 200 to nearly 460 mM NaCl over the same pH range. At still higher NaCl concentrations, samples completely lose any Bragg scattering, and no reflections are observed.

At salt concentrations below c^*, the Bragg reflection observed for G1-PAMAM/DNA samples shifts to lower Q, or equivalently larger DNA−DNA spacings, but maintain their peak shape with added salt. In contrast, we see significant peak broadening at salt concentrations at or above c^*. This peak broadening at high salt concentration is shown for G1-PAMAM/DNA at two different pHs in Figure 5. Here we plot the normalized SAXS scattering intensity (I/I_{max}) as a function of scattering vector Q for G1-PAMAM/DNA condensed at pH 4 and pH 8 under both low and high salt concentrations. For G1-PAMAM/DNA condensed at pH 4, we plot 0 and 525 mM added NaCl concentration. For pH 8, we plot 0 and 250 mM added NaCl concentration, where 250 mM NaCl is already above c^* for this system. Once above c^*, Bragg reflections are observed to simultaneously shift to lower q and broaden with further added salt. Equivalent results are seen in G0-PAMAM/DNA complexes (not shown).

Figure 6 shows we can collapse the salt-dependent phase behavior data for G1-PAMAM dendriplexes for all pHs studied to a single curve. Here, we plot the relative change in the Bragg spacing ($D_{Br}/D_{Br,eq}$) as a function of the added NaCl salt concentration normalized by the crossover salt concentration for each pH/cation system (c/c^*). Here, $D_{Br,eq}$ is the equilibrium Bragg spacing observed without added salt. The slopes at all pHs are quite similar for G1-PAMAM/DNA in both regimes: above and below c^*. As discussed above, the scattering profiles also show significant peak width changes occur at c^*. To quantify this peak broadening, we plot in Figure 6B the average in-plane correlation lengths, ξ, calculated from the full width at half-maximum of the observed Bragg reflections as $\xi = 2\pi/\Delta q_{Br}$, as a function of c/c^*. This correlation length reflects the in-plane, long-range ordering of the DNA helices in the system. Below c^*, there is some variation of ξ between samples, but they remain fairly consistent and independent of pH. Typical values of ξ below c^* range between 220 and 300 Å and do not vary significantly with salt. At or above the critical salt concentration, however, we see a dramatic decrease in the correlation lengths of G1-PAMAM/DNA for all three pHs that decreases continuously with added salt. Eventually sufficient salt is added that no further Bragg scattering is observed. This last regime is indicative of either an isotropic network of DNA and PAMAM forming or complete dissolution of the samples.

DISCUSSION

In vitro condensation of high molecular weight DNA by a variety of multivalent cations has been studied extensively.

dx.doi.org/10.1021/ma5020808 | *Macromolecules* 2014, 47, 8768−8776

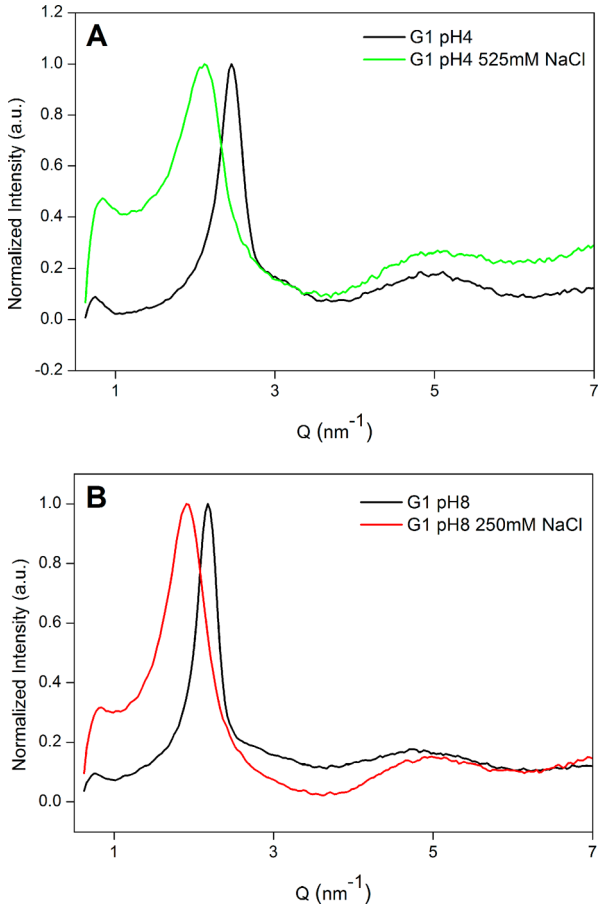

Figure 5. Scattering profiles for G1-DNA assemblies at (A) pH 4 and (B) pH 8 for both low salt and high salt conditions. Shown is the normalized intensity (I/I_{max}) as a function of scattering vector Q.

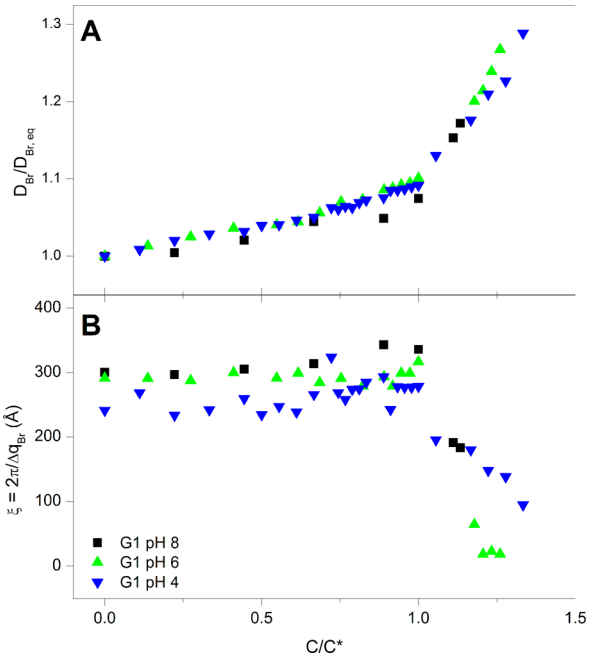

Figure 6. (A) Normalized D_{Br} spacing and (B) in-plane correlation lengths, $\xi = 2\pi/\Delta q_{Br}$, for DNA condensed with G1-PAMAM at different pH as a function of the salt concentration normalized by the critical salt concentration for each system (c/c^*). A discontinuous phase transition occurs at c^* where both the salt sensitivity and the long-range order of the PAMAM/DNA condensed phase are significantly altered.

Spontaneous packaging of DNA into hexagonal arrays typically occurs in the presence of cations with net charge of +3 or higher.[38,39] DNA helices in these packaged arrays do not touch but are separated by ~5−15 Å of water, equivalent to a few monolayers of water.[40] The water present is indicative of a balancing of attractive and repulsive thermodynamic forces within the condensed cation/DNA phase. In the presence of condensing cations, there is a substantial reduction of the repulsive electrostatic interaction between DNA helices. This reduction, however, does not by itself account for the attractive interaction measured, indicating DNA condensation requires more than just counterion condensation.[39] Most current theoretical models therefore require correlation of charges or water structures between DNA helices to account for the magnitude of the experimentally determined attractions stabilizing condensed DNA.[40−44] A convenient means to accomplish such correlations is to presume that cation binding occurs in one of the grooves of the DNA helix, thus coordinating charges, or restructuring the water molecules, along these interfaces. In this model, cations bind in grooves and allow the bound positive charges on one DNA to correlate to negative phosphate backbones on an apposing DNA molecule. Some experimental results suggest that linear cations do indeed bind in the grooves of DNA though it is not clear if this binding is in the major, minor, or both grooves.[45−49]

Hyperbranched molecules, such as dendrimers, present a significant problem for such groove binding models. Even for low generations, the size of the dendrimer already approach or exceed the dimensions of even the major groove of DNA. The major groove in B-DNA is approximately 8.5 Å deep and 12 Å wide. In comparison, G0-PAMAM has a diameter of ~15 Å while G1-PAMAM has a diameter of 22 Å. We would anticipate therefore that PAMAM is not likely capable of coordinating in DNA grooves in the same manner as has been proposed for linear cations. Recently, using osmotic force measurements, we showed that low generation PAMAM dendrimers condense DNA in hexagonally packaged arrays, but their dependence on cation charge at near neutral pH is completely different than comparably charged linear cations.[29] We proposed the differences are likely due to PAMAM using other binding modes, such as cation bridging between DNA double helices, to condense DNA as has been proposed by others theoretically and experimentally.[16,23,50]

In this paper, we are interested in understanding the effect of pH on the intermolecular forces in DNA condensed by low generation PAMAM and the resulting phase behavior and salt stabilities of the complexes. Our earlier experiments showed that condensing DNA with PAMAM at a specific pH alters DNA packaging more strongly than changing the pH after dendriplex formation.[29] These results most likely suggest that the pK_as of the PAMAM amines, once bound, are shifted and their ability to protonate or deprotonate are different than unbound PAMAM in solution. To keep samples as uniform as possible, we have made all the samples here by first pH buffering the DNA and the dendrimer separately and then mixing the solutions to condense at the desired pH. After condensation, samples were maintained at the same pH with 10 mM buffer solutions.

The ability for G0- and G1-PAMAM to spontaneously condense DNA at all pHs in our experiments is consistent with

dx.doi.org/10.1021/ma5020808 | Macromolecules 2014, 47, 8768−8776

the net valency exceeding +3 in all the samples. As discussed in the Results section, G0 is estimated to be +3.5 to +5.1 and G1 is estimated to be +7 to +13 over the pH range of 8 to 4. At equilibrium (i.e., $\Pi = 0$), we see a pH-dependent interaxial spacing (D_{eq}) for both PAMAM/DNA systems. As DNA has a 2 nm diameter, these interaxial spacings indicate ∼10.1−11.6 Å of water for G0-PAMAM/DNA and ∼9.7−13.5 Å of water between helices in G1-PAMAM/DNA depending on the pH. All of these spacings are smaller than the G0- and G1-PAMAM molecule diameters in solution. While large generation dendrimers are thought to have spherical shapes, low generation dendrimers are believed to be more disk-like in shape.[51] This molecule shape may allow G0 and G1 to condense DNA to spacings smaller than the PAMAM diameters.

We previously showed that homologous linear cations, such as alkylamines, arginines, or lysines, converge at high osmotic pressure to the same repulsive limit regardless of cation length or charge for a given cation species.[32,33] The magnitude of the repulsions however changed with cation chemistry. The attractions in all these linear cationic systems were shown to have a similar $\sim 1/N$ dependence, where N is the charge of the polycation. We argued the $1/N$ dependence likely arises from translational entropy of the bound cations where, for example, there is less loss of entropy in correlating one +3 counterion than three +1 ions. Although the chemistries of G0- and G1-PAMAM are essentially identical, we observe here by force measurements that at near neutral pH the different PAMAM/DNA complexes do not converge to the same repulsive limit. If we compare the data for pH 7.5 given in Table 1, we see that the measured attractions for the two PAMAM generations are nearly identical despite G1-PAMAM being +8 and G0-PAMAM being +4 at this pH. Repulsions, however, are larger for G1-PAMAM/DNA. Combined, these forces result in G1-PAMAM/DNA being more loosely packaged than G0-PAMAM/DNA at neutral pH despite being more highly charged—directly opposite to what is observed for homologous linear cations.

Focusing on the effect of pH on the forces, we see that for a given dendriplex system, despite starting at very different interaxial spacings at equilibrium, both G0- and G1-PAMAM condensed DNA converge to the same high pressure limit for all pHs studied as shown in Figures 1 and 2. This convergence is better in G0-PAMAM/DNA than in G1-PAMAM/DNA complexes, perhaps reflecting increased steric effects in the larger generation dendrimer. Using the estimates of residual net charge, we can also determine the dependence of the attractive and repulsive free energy contributions for the PAMAM dendriplexes as a function of the inverse dendrimer charge N (Figure 3). For both dendriplex systems, the respective ΔG_R are relatively insensitive to pH and show little dependence (<4%) on dendrimer charge. The magnitude of the short-range repulsive force in DNA condensed by G1-PAMAM is seen to be ∼15% higher than G0-PAMAM at all pHs. In contrast, the attractions vary significantly with the inverse charge of the dendrimer, comparable to attractions observed for linear DNA condensing agents. Over the pH range of 8 to 4, ΔG_A values are seen to increase ∼24% for G0-PAMAM and ∼50% for G1-PAMAM. Surprisingly, the magnitudes of the attractions are quite similar for G0 and G1 over pH 6 to 8 despite large differences in the net charge of the two dendrimers. Ultimately, G1-PAMAM does have a greater change in the attractions, and we observe that at pH 4 the increased attractions allow G1-PAMAM for the first time to condense DNA more tightly than G0-PAMAM at the same pH. It is interesting to note that extrapolating the force data suggests that, while trivalent or higher is typically sufficient to condense DNA, an approximately +5 G1-PAMAM would not be able to condense DNA primarily due to the weak attractions of the hyperbranched dendrimer compared to similarly charged linear or inorganic cations. How exactly the dendrimer molecules are arranged within the condensed phase still remains to be determined.

The salt dependence of the DNA−DNA spacings without applied pressure was also determined for G0- and G1-PAMAM dendriplexes condensed at different pHs (Figure 4). For all systems, added NaCl salt causes the DNA packaging to swell, resulting in larger spacings. We previously observed that salt dependencies in protamine−DNA are highly dependent on the salt species, not just charge.[52] Added salt does not simply screen electrostatic attractions in the cation condensed DNA phase but acts through some complicated combination of electrostatic screening, anion binding to the bound cation, and/or cation competition with the bound cation for DNA binding. Here, for PAMAM condensed DNA, we see large changes in the DNA−DNA spacings increasing as much as 7.5 Å for G1-PAMAM/DNA with added NaCl salt (Figure 4D). There are also two unique salt regimes observed for both PAMAM/DNA systems. At low salt, with DNA packaged tightly in a hexagonal array, we observe a slow swelling regime. Then at a specific critical salt concentration, c^*, a phase transition occurs, and a much faster rate of swelling is observed with additional added salt. Both the rate of swelling and c^* magnitude depend on the PAMAM generation number and the pH at condensation. Significantly higher NaCl concentration is needed to induce the discontinuous phase transition with PAMAM/DNA condensed at low pH compared to high pH. Also, the more highly charged G1-PAMAM/DNA results in higher c^* for all pHs compared to G0-PAMAM/DNA.

Scattering profiles before and after c^* are consistent with a salt-induced melting transition (Figure 5). Before c^*, sharp Bragg reflections are observed to maintain their sharpness but shift to lower Q, or equivalently larger DNA−DNA spacings, with added salt. At c^*, the observed Bragg reflections are significantly broader. Above c^*, these broad reflections simultaneously shift to lower Q and broaden with further added salt. These results suggest a discontinuous phase transition occurring at c^* from a tightly packaged hexagonal DNA array at low salt to a more loosely organized, fluctuation dominated phase above c^*—most likely a cholesteric liquid crystalline phase. The cholesteric phase of DNA observed at high salt is characterized by increased positional disorder and greater sensitivity to configuration fluctuations with added salt. Eventually, enough salt is added to disrupt DNA order sufficiently that all Bragg scattering is lost. Because of the relatively high concentration of DNA and cation in our X-ray samples, this likely is an isotropic network phase of PAMAM and DNA chains forming at high salt. Similar salt-dependent phase transitions were observed for linear cation/DNA complexes including polylysine, polyarginine, and spermidine.[53,54] For the linear cations, the critical salt concentrations were highly dependent on the nature of the cation used to condense DNA. In our study, the chemical makeup of our two PAMAM systems are nearly identical; thus, the observed differences in c^* are most likely resulting from differences in the net charge of the dendrimer and the ability of the monovalent salt to compete with the polyvalent PAMAM molecules. The

dx.doi.org/10.1021/ma5020808 | Macromolecules 2014, 47, 8768−8776

hexagonal−cholesteric transition, however, is likely a complicated combination of chain configurational entropy and ion-binding competition that is not easily understood. Recently, similar phase transitions between a square, a hexagonal, and a "bead on a string" phase were reported for G4-PAMAM/DNA as a function of the charge ratio of amines to phosphates and the degree of protonation (dp).[26] In these samples, dp was adjusted after complex formation by addition of concentrated acid or base.

Lastly, we show that we can collapse all of the G1-PAMAM/DNA salt data to a single curve by plotting the relative increase in Bragg spacing ($D_{Br}/D_{Br,eq}$) as a function of the salt concentration normalized by the critical salt concentration (c/c^*) for each pH/salt system. Similar results are seen with G0-PAMAM/DNA (not shown). This universal behavior suggests that there is a common physical origin for the observed discontinuous phase transition that is independent of pH for a given PAMAM/DNA system. Despite each G1-PAMAM/DNA starting from its own unique pH-dependent packaging state without added salt, we unexpectedly see all three pH samples swell ∼10% from their original Bragg spacing before reaching the salt-induced melting transition at c^* to a more loosely ordered array. Once above c^*, G1-PAMAM condensed at pH 8 swells an additional 20%, while G1-PAMAM dendriplexes condensed at pH 4 and 6 swell approximately 30% more before Bragg reflections are lost. The average in-plane correlation lengths, ξ, also change dramatically at c^*. Below c^*, G1-PAMAM has correlation lengths ξ of ∼220−300 Å (or approximately 7−10 DNA repeats) for all three pHs. Near c^* we observe ξ quickly drops to just a few DNA repeats for all the samples. Once in the fluctuation dominated cholesteric phase, the PAMAM/DNA is increasingly sensitive to monovalent salt and the complex opens up quickly, becoming highly disordered until all Bragg scattering is lost.

CONCLUSIONS

In this paper, we describe the role of pH on the packaging, compaction energies, and phase behavior for DNA condensed by low generation PAMAM dendrimers. At equilibrium, in low salt conditions, all samples are consistent with DNA being locally hexagonally packaged by the PAMAM dendrimers. Using osmotic stress, we have directly measured the intermolecular forces in G0- and G1-PAMAM/DNA condensates as a function of pH at condensation. By separating and quantifying the attractive and repulsive free energy contributions, we show that repulsions for a given PAMAM generation are nearly unaffected by pH while the observed attractions scale approximately linearly with the inverse of the dendrimer charge. Changes in the pH at condensation also greatly influence the resulting phase behavior for PAMAM dendriplexes. For all systems, a hexagonal to cholesteric phase transition is observed with the addition of monovalent salt. The critical salt concentration, c^*, required to induce this melting transition is observed to be dependent on both PAMAM generation number and the pH at condensation. Together, our results suggest that pH and salt play a central role in tuning the intermolecular forces and packaging within the PAMAM/DNA condensed phase. The ability to manipulate these forces are essential for therapeutic uses of PAMAM, such as successful gene delivery.

AUTHOR INFORMATION

Corresponding Author

*(J.E.D.) E-mail: derouchey@uky.edu.

Notes

The authors declare no competing financial interest.

ACKNOWLEDGMENTS

This research was financially supported by start-up funds from the University of Kentucky and the University of Kentucky Research Challenge Trust Fund (RCTF) Fellowship for Biochemistry.

REFERENCES

(1) Kay, M. A.; Glorioso, J. C.; Naldini, L. *Nat. Med.* **2001**, *7* (1), 33−40.
(2) Yin, H.; Kanasty, R. L.; Eltoukhy, A. A.; Vegas, A. J.; Dorkin, J. R.; Anderson, D. G. *Nat. Rev. Genet.* **2014**, *15* (8), 541−555.
(3) Thomas, C. E.; Ehrhardt, A.; Kay, M. A. *Nat. Rev. Genet.* **2003**, *4* (5), 346−358.
(4) Niidome, T.; Huang, L. *Gene Ther.* **2002**, *9* (24), 1647−1652.
(5) Pack, D. W.; Hoffman, A. S.; Pun, S.; Stayton, P. S. *Nat. Rev. Drug Discovery* **2005**, *4* (7), 581−593.
(6) Garnett, M. C. *Crit. Rev. Ther. Drug Carrier Syst.* **1999**, *16* (2), 147−207.
(7) Bielinska, A. U.; Chen, C.; Johnson, J.; Baker, J. R. *Bioconjugate Chem.* **1999**, *10* (5), 843−850.
(8) Eichman, J. D.; Bielinska, A. U.; Kukowska-Latallo, J. F.; Baker, J. R., Jr. *Pharm. Sci. Technol. Today* **2000**, *3* (7), 232−245.
(9) Dufès, C.; Uchegbu, I. F.; Schätzlein, A. G. *Adv. Drug Delivery Rev.* **2005**, *57* (15), 2177−2202.
(10) Nguyen, T. T.; Shklovskii, B. I. *J. Chem. Phys.* **2001**, *115* (15), 7298−7308.
(11) Kunze, K. K.; Netz, R. R. *Phys. Rev. Lett.* **2000**, *85* (20), 4389−4392.
(12) Qamhieh, K.; Nylander, T.; Ainalem, M.-L. *Biomacromolecules* **2009**, *10* (7), 1720−1726.
(13) Tian, W.-d.; Ma, Y.-q. *Macromolecules* **2010**, *43* (3), 1575−1582.
(14) Mogurampelly, S.; Nandy, B.; Netz, R.; Maiti, P. *Eur. Phys. J. E* **2013**, *36* (6), 1−9.
(15) Qamhieh, K.; Nylander, T.; Black, C. F.; Attard, G. S.; Dias, R. S.; Ainalem, M. L. *Phys. Chem. Chem. Phys.* **2014**, *16* (26), 13112−13122.
(16) Evans, H. M.; Ahmad, A.; Ewert, K.; Pfohl, T.; Martin-Herranz, A.; Bruinsma, R. F.; Safinya, C. R. *Phys. Rev. Lett.* **2003**, *91* (7), 075501.
(17) Liu, Y.-C.; Chen, H.-L.; Su, C.-J.; Lin, H.-K.; Liu, W.-L.; Jeng, U. S. *Macromolecules* **2005**, *38* (23), 9434−9440.
(18) Dootz, R.; Toma, A. C.; Pfohl, T. *Soft Matter* **2011**, *7* (18), 8343−8351.
(19) Pfohl, T.; Otten, A.; Köster, S.; Dootz, R.; Struth, B.; Evans, H. M. *Biomacromolecules* **2007**, *8* (7), 2167−2172.
(20) Ainalem, M.-L.; Nylander, T. *Soft Matter* **2011**, *7* (10), 4577−4594.
(21) Carnerup, A. M.; Ainalem, M.-L.; Alfredsson, V.; Nylander, T. *Soft Matter* **2011**, *7* (2), 760−768.
(22) Froehlich, E.; Mandeville, J. S.; Weinert, C. M.; Kreplak, L.; Tajmir-Riahi, H. A. *Biomacromolecules* **2010**, *12* (2), 511−517.
(23) Ritort, F.; Mihardja, S.; Smith, S. B.; Bustamante, C. *Phys. Rev. Lett.* **2006**, *96* (11), 118301.
(24) Fant, K.; Esbjörner, E. K.; Lincoln, P.; Nordén, B. *Biochemistry* **2008**, *47* (6), 1732−1740.
(25) Yu, S.; Li, M. H.; Choi, S. K.; Baker, J. R.; Larson, R. G. *Molecules* **2013**, *18* (9), 10707−10720.
(26) Yang, C.-C.; Huang, Y.-C.; Chen, C.-Y.; Su, C.-J.; Chen, H.-L.; Ivanov, V. A. *Macromolecules* **2014**, *47* (9), 3117−3127.

(27) Su, C.-J.; Chen, C.-Y.; Lin, M.-C.; Chen, H.-L.; Iwase, H.; Koizumi, S.; Hashimoto, T. *Macromolecules* **2012**, *45* (12), 5208−5217.
(28) Shifrina, Z. B.; Kuchkina, N. V.; Rutkevich, P. N.; Vlasik, T. N.; Sushko, A. D.; Izumrudov, V. A. *Macromolecules* **2009**, *42* (24), 9548−9560.
(29) An, M.; Parkin, S. R.; DeRouchey, J. E. *Soft Matter* **2014**, *10* (4), 590−599.
(30) Rau, D. C.; Parsegian, V. A. *Biophys. J.* **1992**, *61* (1), 246−259.
(31) Todd, B. A.; Adrian Parsegian, V.; Shirahata, A.; Thomas, T. J.; Rau, D. C. *Biophys. J.* **2008**, *94* (12), 4775−4782.
(32) DeRouchey, J.; Parsegian, V. A.; Rau, D. C. *Biophys. J.* **2010**, *99* (8), 2608−2615.
(33) DeRouchey, J.; Hoover, B.; Rau, D. C. *Biochemistry* **2013**, *52* (17), 3000−3009.
(34) McGhee, J. D.; Wood, W. I.; Dolan, M.; Engel, J. D.; Felsenfeld, G. *Cell* **1981**, *27* (1, Part 2), 45−55.
(35) Parsegian, V. A.; Rand, R. P.; Fuller, N. L.; Rau, D. C. Osmotic stress for the direct measurement of intermolecular forces. In *Methods in Enzymology*; Lester, P., Ed.; Academic Press: New York, 1986; Vol. *127*, pp 400−416.
(36) DeRouchey, J. E.; Rau, D. C. *J. Biol. Chem.* **2011**, *286* (49), 41985−41992.
(37) Cakara, D.; Kleimann, J.; Borkovec, M. *Macromolecules* **2003**, *36* (11), 4201−4207.
(38) Bloomfield, V. A. *Curr. Opin. Struct. Biol.* **1996**, *6* (3), 334−341.
(39) Bloomfield, V. A. *Biopolymers* **1997**, *44* (3), 269−282.
(40) Stanley, C.; Rau, D. C. *Curr. Opin. Colloid Interface Sci.* **2011**, *16* (6), 551−556.
(41) Kornyshev, A. A.; Lee, D. J.; Leikin, S.; Wynveen, A. *Rev. Mod. Phys.* **2007**, *79* (3), 943−996.
(42) Kornyshev, A. A.; Leikin, S. *Proc. Natl. Acad. Sci. U. S. A.* **1998**, *95* (23), 13579−13584.
(43) Kornyshev, A. A.; Leikin, S. *Phys. Rev. Lett.* **1999**, *82* (20), 4138−4141.
(44) Mills, M.; Orr, B. G.; Banaszak Holl, M. M.; Andricioaei, I. *J. Phys. Chem. B* **2012**, *117* (4), 973−981.
(45) Fita, I.; Campos, J. L.; Puigjaner, L. C.; Subirana, J. A. *J. Mol. Biol.* **1983**, *167* (1), 157−177.
(46) Feuerstein, B. G.; Pattabiraman, N.; Marton, L. J. *Nucleic Acids Res.* **1990**, *18* (5), 1271−1282.
(47) Hud, N. V.; Milanovich, F. P.; Balhorn, R. *Biochemistry* **1994**, *33* (24), 7528−7535.
(48) Ruiz-Chica, J.; Medina, M. A.; Sanchez-Jimenez, F.; Ramirez, F. J. *Biophys. J.* **2001**, *80* (1), 443−454.
(49) Ouameur, A. A.; Tajmir-Riahi, H. A. *J. Biol. Chem.* **2004**, *279* (40), 42041−42054.
(50) Podgornik, R.; Ličer, M. *Curr. Opin. Colloid Interface Sci.* **2006**, *11* (5), 273−279.
(51) Lee, I.; Athey, B. D.; Wetzel, A. W.; Meixner, W.; Baker, J. R. *Macromolecules* **2002**, *35* (11), 4510−4520.
(52) DeRouchey, J. E.; Rau, D. C. *J. Phys. Chem. B* **2011**, *115* (41), 11888−11894.
(53) DeRouchey, J.; Netz, R. R.; Radler, J. O. *Eur. Phys. J. E* **2005**, *16* (1), 17−28.
(54) Yang, J.; Rau, D. C. *Biophys. J.* **2005**, *89* (3), 1932−1940.